Biophysical Characterization of Iron in Mitochondria Isolated from Respiring and Fermenting Yeast

ARTICLE *in* BIOCHEMISTRY · JULY 2010

Impact Factor: 3.02 · DOI: 10.1021/bi100558z · Source: PubMed

6 AUTHORS, INCLUDING:

Gregory Holmes-Hampton
National Institutes of Health
12 PUBLICATIONS **153** CITATIONS

SEE PROFILE

Yisong Guo
Carnegie Mellon University
31 PUBLICATIONS **492** CITATIONS

SEE PROFILE

Published in final edited form as:
Biochemistry. 2010 July 6; 49(26): 5436–5444. doi:10.1021/bi100558z.

Biophysical Characterization of Iron in Mitochondria Isolated from Respiring and Fermenting Yeast†

Jessica Garber-Morales[1], **Gregory P. Holmes-Hampton**[1], **Ren Miao**[1], **Yisong Guo**[2], **Eckard Münck**[2], and **Paul A. Lindahl**[1,3]

[1] Department of Chemistry, Texas A&M University, College Station, TX 77843-3255

[2] Department of Chemistry, Carnegie Mellon University, Pittsburgh, PA 15213

[3] Department of Biochemistry and Biophysics, Texas A&M University, College Station, TX 77843

Abstract

The distributions of Fe in mitochondria isolated from respiring, respiro-fermenting, and fermenting yeast cells were determined by an integrative biophysical approach involving Mössbauer and electronic absorption spectroscopies, EPR and ICP-MS. Approximately 40% of the Fe in mitochondria from respiring cells was present in respiration-related proteins. The concentration and distribution of Fe in respiro-fermenting mitochondria, where both respiration and fermentation occur concurrently, was similar to that of respiring mitochondria. The concentration of Fe in fermenting mitochondria was also similar, but the distribution differed dramatically. Here, respiration-related Fe-containing proteins were diminished *ca*. 3-fold, while nonheme HS Fe^{II} species, nonheme mononuclear HS Fe^{III}, and Fe^{III} nanoparticles dominated. These changes were rationalized by a model in which the pool of nonheme HS Fe^{II} ions serves as feedstock for Fe/S cluster and heme biosynthesis. The absolute concentrations of respiration-related protein complexes were estimated.

Mitochondria are cellular organelles that play critical roles in cellular physiology. Respiration and oxidative phosphorylation occur in these organelles, as do heme biosynthesis and iron/sulfur cluster assembly. As such, mitochondria are “hubs” of cellular iron trafficking (3). The Fe^{II} ions used for these processes are imported by Mrs3p and Mrs4p, high-affinity transporters on the IM (3). Once in the matrix, these ions are delivered to Fe/S scaffold proteins and ferrochelatase (3). Many of these Fe/S and heme centers are inserted into respiratory complexes. Succinate dehydrogenase contains one $[Fe_2S_2]$, $[Fe_3S_4]$, and $[Fe_4S_4]$ cluster each as well as a LS heme *b* (4). Cytochrome bc_1 contains 2 LS *b* type hemes, 1 LS *c* heme, and a Rieske $[Fe_2S_2]$ cluster (5). Cytochrome *c* contains 1 LS heme *c*. Cytochrome *c* oxidase contains 2 heme *a* and 3 Cu ions(6). Other mitochondrial proteins contain $[Fe_4S_4]$, $[Fe_2S_2]$ clusters, hemes and nonheme Fe^{II} ions (see (1) for a list of mitochondrial Fe-containing proteins).

†This study was supported by the National Institutes of Health grants GM084266, (PAL), EB-001475 (EM), T32GM008523 (GPHH and JGM) and by the Robert A. Welch Foundation (A1170, PAL).

*To whom correspondence should be addressed: Phone: 979-845-0956; FAX: 979-845-4719; lindahl@chem.tamu.edu.

Supporting Information Available: Table S1, Protein and metal concentrations in isolated mitochondria; Figure S1, Electronic absorption spectra of heme-containing proteins; Figure S2, Protection of cytochrome *c* from protease degradation in isolated mitochondria; Figure S3, Mössbauer spectra of a respiring mitochondrial batch not shown in Figure 2 but used in constructing Table 1; Figure S4, Electronic absorption spectra of respiring mitochondria suspensions; Table S2, Concentrations of each heme component determined for individual mitochondrial samples; Figure S5, 10 K EPR spectra of mitochondria batches not shown in Figure 4 but used in the construction of Table 1; Figure S6, electronic absorption spectra of different batches of fermenting mitochondria. This material is available free of charge via the Internet at http://pubs.acs.org.

Mitochondrial dysfunction is associated with various diseases, including aging, cancer, heart disease, anemia and neurodegeneration (7–9). As cells age, there is a decline in Fe/S cluster biogenesis and mitochondrial membrane potential, leading with higher probability to a cellular crisis associated with loss of mitochondrial DNA, the instability and hypermutability of nuclear DNA, and cancer (10). Aged cells exhibit signs of iron starvation (10). Reactive Oxygen Species (ROS) generated by Fe centers within the mitochondria may damage the DNA and other cellular components (11) causing apoptosis (12–14). Ferrous ions are particularly adept at producing ROS via Fenton Chemistry (15). In Friedreich's Ataxia, mitochondrial frataxin is depleted causing a build-up of iron in the organelle (16–19). In Parkinson's disease, there is a build-up of Fe in the *substantia nigra* portion of the brain (20–21). Patients with Sideroblastic anemia accumulate Fe that cannot incorporate into hemoglobin (3,22).

Much progress in understanding cellular function has been made by "omics"-level studies in which entire subsets of cellular components are measured simultaneously and analyzed as a system (23). We have developed an integrative biophysical approach centered on Mössbauer spectroscopy to study the systems-level distribution of iron within cells and organelles (2). ^{57}Fe Mössbauer spectroscopy detects *all* Fe species in a sample, with spectral intensities proportional to relative Fe concentrations (24). In complex systems, Mössbauer can generally not resolve *individual* Fe species, but it can identify *groups*. This is not ideal, but the resolution of Fe species can be enhanced by EPR, which can detect paramagnetic species, electronic absorption spectroscopy, which can quantify heme chromophores, and ICP-MS, which can quantify the overall Fe concentration.

In this study, we have assessed the Fe content of mitochondria isolated from yeast grown under fermenting, respiro-fermenting and respiring conditions. Mitochondria play a dominant role in respiration but not fermentation; however, they are essential for cell viability regardless of metabolic growth mode. Fermenting cells produce fewer mitochondria than respiring cells. Early in exponential growth phase, fermenting cells are largely devoid of mitochondria; in later stages, the organelle occupies ~3% of cell volume (25). Under respiration, mitochondria represent ~10% of cell volume. Mitochondria in yeast are present as a large tubular network (26); the network from fermenting cells is thinner and less branched.

We report here that respiration-related Fe-containing proteins and other $[Fe_4S_4]^{2+}$ cluster-containing proteins dominate the iron content of mitochondria from respiring and respiro-fermenting cells. Under fermention, the concentrations of these species decline while those of nonheme high-spin (NHHS) Fe^{II} ions, mononuclear HS Fe^{III} ions and Fe^{III} nanoparticles increase. These changes can be rationalized by assuming that the NHHS Fe^{II} ions constitute a pool used for Fe/S cluster and heme biosynthesis.

Experimental Procedures

Twenty five L cultures of W303-1B cells were grown on minimal media (27) with 3% v/v glycerol (batches R1, R2, R4, R5), 2% w/v galactose (batches RF1, RF2), or 2% w/v glucose (batches F5 – F16). See Table S1 for a listing of all batches used in this study. Respiring batches were supplemented with 10% YPG medium except for R3 (grown on YPG) and F1–F4 (grown on YPD (28)). Batches were supplemented with 40 μM ^{57}Fe as described (27) except RF1 which was supplemented with 20 μM ^{57}Fe. Mitochondria were isolated, packed, and frozen in the as-isolated state, as described (1–2), without adding reductants or oxidants. In our current samples, dithionite had less ability to reduce spectral components, relative to the effect reported previously (1). See (29) for current Mössbauer spectra of dithionite-treated mitochondria. In earlier batches, dithionite reduced the Fe in

about half of the *central* doublet whereas in our current samples, dithionite had little effect (As the *central* quadrupole doublet comprises low-spin Fe(II) hemes and $[Fe_4S_4]^{2+}$ clusters, dithionite would act on the latter). We are uncertain why our samples have become insensitive to dithionite, but we suspect that the negatively charged dithionite ion cannot cross the IM, suggesting that only mitochondria with broken membranes can be reduced. In our current samples a higher proportion of membranes may be intact. Intactness was evaluated by protease protection assays as described (30).

Protein and metal concentrations were determined as described (1) except that 1–2% deoxycholate was used to disrupt membranes, and the bicinchoninic acid method (Thermo Scientific) was used for protein concentrations. The protein concentrations of packed mitochondria reported in the current study were higher by a factor of ~ 2 relative to our previous determinations (1). Current samples were treated with deoxycholate rather than being sonicated prior to protein concentration determinations, and this may have released additional proteins from membranes and/or reduced the extent of protein degradation. The current metal/protein ratios (~ 4 nmol Fe/mg protein) for respiring and respirofermenting mitochondria are similar to those reported from other labs(16,31–34), and thus we consider our current protein concentrations to be more accurate.

EPR and Mössbauer measurements were performed as described (1,27). For electronic absorption spectroscopy, samples were resuspended in 0.6 M sorbitol, 20 mM HEPES, pH 7.4; spectra were obtained as described (2). Spectra of human cytochrome b_5 (Sigma, 18 μM in a buffer composed of 1.2 M sorbitol, 50 mM Tris pH 8.5 plus 1 mM dithionite) and yeast cytochrome *c* (Sigma, 20 μM in the same buffer) were also collected. The digital spectrum of bovine heart cytochrome *c* oxidase (35) was provided by Dr. Graham Palmer (Rice University). Absorbances were normalized to a 1 cm pathlength, and divided by molar protein concentrations. Extinction coefficients for cytochrome *c* oxidase were divided by 2 to account for there being 2 heme *a* groups per protein. The resulting wavelength-dependent extinction coefficients ($\varepsilon_a(\lambda)$, $\varepsilon_b(\lambda)$ and $\varepsilon_c(\lambda)$) for heme *a*, *b* and *c*, respectively, are shown in Figure S1. Spectra were analyzed using OriginPro (www.originlab.com) and the relationship

$$\mathrm{Abs}(\lambda)=[\mathrm{Heme}\,a]\,\varepsilon_a(\lambda)+[\mathrm{Heme}\,b]\,\varepsilon_b(\lambda)+[\mathrm{Heme}\,c]\,\varepsilon_c(\lambda)+\text{light scattering}$$

where [Heme *x* = *a*, *b*, or *c*] is the concentration of each heme center in the mitochondrial suspension. Concentrations were adjusted manually to obtain the composite spectra shown in Figure 3, using parameters in Table 1.

Results

Respiring mitochondria

Western blots of mitochondria isolated from respiring cells showed a 10-fold enrichment of the mitochondrial porin relative to that in cell extracts (Figure 1). Since ~ 10% of the volume of respiring yeast cells is due to mitochondria (25), this indicates that our samples were relatively pure. The membranes of isolated mitochondria were largely intact, in that the IMS protein cytochrome *c* was protected from Proteinase K-catalyzed hydrolysis unless deoxycholate was added to disrupt membranes (Figure S2). The metal content of samples was determined by ICP-MS (averages in Table 1, individual determinations in Table S1). Low-field Mössbauer spectra of respiring mitochondria were dominated by the *central doublet* (Figure 2C, blue line). This doublet (60% of Fe, Table 1) has $\delta \approx 0.45$ mm/s and $\Delta E_Q \approx 1.15$ mm/s, parameters characteristic of both S = 0 $[Fe_4S_4]^{2+}$ clusters and LS Fe^{II} hemes. A minor contribution of S = 0 $[Fe_2S_2]^{2+}$ clusters to the central spectral region could

not be excluded; fits for the 0.05 T spectra, but not the 8.0 T spectra were improved by assuming that ~ 5% of total Fe was in this form (with $\delta = 0.27$ mm/s, $\Delta E_Q = 0.55$ mm/s).

Respiring mitochondria exhibited a quadrupole doublet with $\delta \approx 0.83$ mm/s, $\Delta E_Q \approx 2.4$ mm/s, typical of HS Fe^{II} hemes (36). The dashed line above the spectrum of Figure 2A is a simulation of this species; the low-energy line is buried under the central doublet. The spectrum also contains paramagnetic feature best recognized by removing the heme and central doublets. The resulting absorption features (Figure 2B) at ~ +3.1 mm/s and ~ −2.7 mm/s strongly suggest S = ½ $[Fe_2S_2]^{1+}$ clusters (due to the Rieske center in the bc_1 complex and the center in succinate dehydrogenase). Assuming the parameters of the Rieske protein (37) to simulate the contribution of a generic S = ½ $[Fe_2S_2]^{1+}$ cluster suggests that ~ 13% of the Fe in respiring mitochondria are present as such clusters. Analysis of Mössbauer and EPR spectra of another batch (R2, Figures S3, 4A and S5) both yielded ~30 μM for this cluster type. At 100 K (Figure 2C) the spin relaxation of the $[Fe_2S_2]^{1+}$ clusters is sufficiently fast to collapse the magnetic pattern observed at 4.5 K, revealing that ≥ 2% of spectral intensity arises from NHHS Fe^{II} species ($\Delta E_Q \approx 3.0$ mm/s, $\delta \approx 1.3$ mm/s). The black line on the 8.0 T data of Figure 2D simulates the central doublet and S = ½ $[Fe_2S_2]^{1+}$ clusters. After subtracting the above-mentioned spectral features, some unresolved absorption remains at the center of the spectrum (Figure 2B) which could not be assigned unequivocally: a portion may be Fe^{III} phosphate nanoparticles.

We previously reported that ~22% of total Fe was present as nonheme Fe^{II} in respiring mitochondria grown on lactate (1). We now suspect that the majority of this was adventitious, as we no longer observe such features with this intensity in spectra of respiring mitochondria. Also, previously reported spectra (1) did not include a HS heme doublet, as we observe currently. In the initial stages of this project, samples were not isolated as rapidly as they are currently, and there may have been some heme and/or Fe/S cluster degradation that led to more intense nonheme HS Fe^{II} doublets.

Mitochondrial suspensions are turbid, leading to electronic absorption spectra with strong sloping baselines due to light scattering (Figure 3). Superimposed on this are Soret bands in the 400 nm region and α and β bands in the 500 – 620 nm region arising from both HS and LS Fe^{II} hemes (35). Spectra of respiring mitochondria were simulated (dashed lines, Figures 3A and S4) by adding spectra of individual heme *a*, *b* and *c* containing proteins (Figure S1). Resulting concentrations (Tables 1 and S2) reveal the dominance of heme *c*, with hemes *b* and *a* present in roughly equal amounts. The HS fraction of these Fe^{II} hemes affords the heme Mössbauer doublet mentioned above, while the LS portion contributes to the central doublet.

EPR spectra of respiring mitochondria revealed additional details of the paramagnetic species observed by Mössbauer spectroscopy. The low-field region (Figure 4D) was dominated by EPR signals at g ≈ 6.0 (E/D = 0) and at g = 6.4 and 5.4 (E/D ≈ 0.021); average spin concentrations are listed in Table 1. We assign these signals to the {a_3:Cu_b} center of cytochrome *c* oxidase in which heme a_3 is Fe^{III} and Cu_b is Cu^I (6). The g = 2 region (Figure 4A) was dominated by signals with $g_{ave} = 1.95$ (2.03, 1.93, 1.91), $g_{ave} = 1.90$ (2.02, 1.90, 1.78), $g_{ave} = 2.02$ (2.08, 1.99, 1.97), and a nearly isotropic signal with g_{ave} = 2.01 (perhaps combined with another signal at g = 2.00) (1). The dashed line in Figure 4A is the composite simulation. The $g_{ave} = 1.95$ and 1.90 signals, respectively, have been assigned to the $[Fe_2S_2]^{1+}$ clusters in succinate dehydrogenase (38) and the Rieske protein of cytochrome bc_1 (1, 39). The $g_{ave} = 2.01$ signal may originate from an S = ½ $[Fe_3S_4]^{1+}$ cluster, arising perhaps from the cluster in succinate dehydrogenase. The signal at g = 2.00 probably arises from an organic-based radical. The $g_{ave} = 2.02$ feature may arise from ET flavoprotein-ubiquinone oxidoreductase (40). Minor resonances between g = 2.2 – 2.1 are

often observed but remain unassigned. The bulk of the spin concentration in the g = 2 region belongs to $[Fe_2S_2]^{1+}$ clusters that are most evident in Mössbauer spectra. The remainder belongs to minor species that may account for the unresolved background in the Mössbauer spectra. These results were generally similar to those reported for mitochondria isolated from yeast grown on glucose/lactate (1).

Respiro-fermenting mitochondria

Metal concentrations of mitochondria isolated from respiro-fermenting cells were similar to those of respiring mitochondria, except that the Mn concentration was 2-fold lower (Table 1). Mössbauer spectra (Figure 5) were also similar. Compared to respiring mitochondria, the proportion of Fe present as the central doublet, HS Fe^{II} hemes, and magnetic Fe in respiro-fermenting mitochondria declined slightly, while the percentages of NHHS Fe^{II} and the unassigned absorption in the center of the spectra increased slightly. A minor contribution of NHHS Fe^{II} (~2%) was assessed using the 100 K spectrum of Figure 5B. The presence of unassigned species is evident from the mismatch of the spectrum and simulation (Figure 5A) at ~ 0 mm/s. The 8.0 T spectrum reveals the presence of mononuclear HS Fe^{III} ions (Figure 5C, cyan line). The black line in Figure 5C is a simulation of the diamagnetic Fe associated with the central doublet at low-field, together with a generic S = ½ $[Fe_2S_2]^{1+}$ cluster. EPR of a well-packed sample of the same batch yielded a spin concentration of 57 μM for the sum of the g_{ave} = 1.95 and 1.90 signals, suggesting that ca. 15% of the Fe belongs to $[Fe_2S_2]^{1+}$ clusters. This value is a bit higher than suggested by the Mössbauer data, but differences are within the uncertainties. The electronic absorption spectrum of respiro-fermenting mitochondria (Figure 3B) revealed heme *a*, *b* and *c* concentrations (Table 1) similar to those of respiring mitochondria.

Fermenting mitochondria

Protein and Fe concentrations for fermenting mitochondria (Tables 1) were again similar to those of respiring and respiro-fermenting mitochondria; the protein concentration might be reduced somewhat, but the variability was too high to establish this. The Mn concentration was similar to that in respiro-fermenting mitochondria and substantially lower than in respiring mitochondria. The Cu concentration was ~ 4-fold lower relative to respiring or respiro-fermenting mitochondria. Mössbauer spectra of fermenting mitochondria (Figure 6) are described in detail elsewhere(29); here we summarize that description. The spectra differed substantially from those of respiring or respiro-fermenting mitochondria in that there was a substantial decline in the fraction of Fe associated with the central doublet and an increase in the proportion of NHHS Fe^{II} and Fe^{III} nanoparticles (δ = 0.52 mm/s, ΔE_Q = 0.63 mm/s). Electronic absorption spectra (Figures 3C and S6) exhibited lower concentrations of heme centers (Tables 1 and S2), consistent with the decline of the HS Fe^{II} heme doublet in Mössbauer spectra. EPR spectra of fermenting mitochondria (Figure 4, C and F) were qualitatively similar to those of respiring and respiro-fermenting mitochondria, but with lower spin concentrations (Table 1). The g = 6 features, assigned to the partially oxidized a_3:Cu_B site of cytochrome *c* oxidase, declined as expected. Summing spin concentrations of the signals in the g = 2 region suggests that ≤ 3% of Mössbauer spectral intensity should be associated with S = ½ species, a fraction too small to be detected in the presence of increased amounts of NHHS Fe^{II} and ferric nanoparticles.

Discussion

The main objective of this study was to characterize the distribution of the major Fe species in mitochondria isolated from respiring, respiro-fermenting, and fermenting yeast cells. We now integrate the results from the various techniques with the known composition of proteins in mitochondria, beginning with the respiring state. Our data allow an estimate of

the absolute concentration of cytochrome *c* oxidase in the organelle. As few other heme *a* containing proteins are found in mitochondria, the heme *a* concentration essentially reflects twice the cytochrome *c* oxidase concentration. Mitochondrial heme monoxygenase may have substoichiometric amounts of heme *a* bound, but we will assume that this is insignificant. The total Fe^{II} heme *a* concentration in respiring mitochondria (Table 1, top panel) suggests an average concentration of ~ 25 μM for cytochrome *c* oxidase with reduced heme *a* species (Table 1, bottom panel). The absence of EPR signals at g ~ 3 indicates the lack of LS Fe^{III} hemes in respiring mitochondria. Since cytochrome *c* oxidase contains 3 molar equivalents of Cu, ~ 40% of the total Cu in respiring mitochondria should be in this enzyme. Most of the remainder might belong to a Cu^{I} pool (31). The percentage of mitochondrial Cu that we estimate for this pool (~ 60%) is less than the previous estimate (~ 90%). The absence of Cu^{II} EPR signals in our preparations is consistent with a Cu^{I} oxidation state for this pool.

The HS Fe^{II} heme quadrupole doublet of respiring mitochondria should include contributions from heme a_3 and HS heme *b* containing proteins (we are unaware of any HS heme *c* – containing proteins). After subtracting the heme a_3 contribution, the HS heme *b* species in respiring mitochondria (Table 1, bottom panel) are likely to be found in cytochrome *c* peroxidase, catalase and NO oxidoreductase, among others. Subtracting the HS heme *b* concentration from the total heme *b* concentration suggests that the concentration of LS heme *b* species in mitochondria is ~ 30 μM. These chromophores are found in succinate dehydrogenase (1 heme *b*), cytochrome bc_1 (2 heme *b*), and others such as cytochrome b_2 and Cox15p. This can be described by the relationship

$$30\,\mu M = [\text{succinate dehydrogenase}] + 2[\text{cytochrome bc}_1] + \text{others}$$

As the spin concentrations for the g_{ave} = 1.94 and 1.90 EPR signals indicate the concentrations of succinate dehydrogenase (~5 μM) and cytochrome bc_1 (~10 μM), respectively, this relationship implies that most LS heme *b* centers in mitochondria reside in these two respiratory complexes.

The known heme *c* containing proteins in mitochondria include cytochrome c_1 and two isoforms of cytochrome *c*. Removing the cytochrome bc_1 concentration suggests that the collective concentration of the isoforms is ~ 110 μM. This indicates that the heme *a* and *c* contents of respiring mitochondria are dominated by cytochrome *c* oxidase and cytochrome *c*, respectively. The heme *b* content is more evenly distributed between HS and LS, with LS forms dominated by succinate dehydrogenase and cytochrome bc_1. Concentrations in Table 1, bottom panel, were calculated with respect to the entire mitochondrial volume. Since species are located in particular regions of the mitochondria, their regional concentrations will be higher.

Succinate dehydrogenase contains 10 molar equivalents of Fe (1 LS heme *b*, 1 Fe_2S_2 cluster, 1 Fe_3S_4 cluster and 1 Fe_4S_4 cluster), so a concentration of ~ 5 μM for this respiratory complex implies a ~ 50 μM Fe contribution overall. Similarly, cytochrome bc_1 contains 5 molar equivalents of Fe (1 heme c_1, 2 heme *b*, and 1 Fe_2S_2 cluster), also implying a ~ 50 μM overall Fe contribution. Including a 60 μM Fe contribution for cytochrome *c* oxidase and 110 μM for cytochrome *c* reveals that *respiration-related complexes constitute ~ 40% of the iron in respiring yeast mitochondria*.

The central doublet of the Mössbauer spectra of respiring mitochondria includes contributions from $[Fe_4S_4]^{2+}$ clusters and LS Fe^{II} hemes. Table 1 and the relationships mentioned above suggest ~30 μM (LS heme *a*) + ~30 μM (LS heme *b*) + ~120 μM (LS

heme *c*) = ~180 μM LS Fe^{II} hemes. Subtracting this from the central doublet leaves ~ 35% of mitochondrial Fe in the form of S = 0 $[Fe_4S_4]^{2+}$ clusters. This corresponds to ~ 250 μM Fe or to ~ 60 μM of such clusters. Subtracting an additional 5 μM contribution due to the succinate dehydrogenase $[Fe_4S_4]^{2+}$ cluster leaves ~ 55 μM for Fe_4S_4 clusters in other mitochondrial proteins.

Some mitochondrial proteins contain only Fe_4S_4 clusters, some contain only Fe_2S_2 clusters, and some contain both cluster types. We have attempted to fit simulations of oxidized $[Fe_2S_2]^{2+}$ clusters into the Mössbauer spectra of respiring mitochondria but we have no clear evidence for their presence. This suggests for respiring mitochondria that the majority of $[Fe_4S_4]^{2+}$ clusters that are not contained in succinate dehydrogenase reside in proteins that contain *only* $[Fe_4S_4]^{2+}$ clusters.

Respiro-fermenting and fermenting mitochondria were analyzed similarly (Table 1, bottom panel); results are summarized by the bar chart in Figure 7. In general, the total Fe concentration was similar regardless of metabolic mode. Also, the overall distribution of Fe in respiro-fermenting mitochondria was similar to that in respiring mitochondria. In contrast, the Fe distribution in fermenting mitochondria was dramatically different. This suggests that the *repression of respiration* by glucose, rather than the occurrence of fermentation *per se*, is responsible for the major shifts observed in Fe distribution. Thus, we will simplify our further analysis by averaging the Fe distributions observed for respiring and respiro-fermenting mitochondria, and then compare this to the distribution obtained under fermentation.

Viewed in the respiration → fermentation direction, cytochrome *c* oxidase ↓ (declined) 4×, succinate dehydrogenase ↓ 3.8×, cytochrome bc_1 ↓ 2.5×, cytochrome *c* ↓ 2×, LS hemes generally ↓ 2× and $[Fe_4S_4]^{2+}$ containing proteins ↓ 3.5×. The Cu^I pool decreased ↓ 3×. The decline in the size of the Cu^I pool upon shifting from respiration to fermentation contrasts with a previous report (31) that the concentration of this pool is independent of metabolic growth mode. In terms of Fe pools, the NHHS Fe^{II} pool, the mononuclear HS Fe^{III} pool and the Fe^{III} nanoparticles went from nearly undetectable in respiring mitochondria to representing ~ 75% of the Fe in the fermenting organelle. These dramatic changes reflect major differences in the way that Fe is handled by the cell, depending on metabolic mode.

We do not know the location of these pools within mitochondria, but suspect that they are located in the matrix. Nor are the ligands coordinating the Fe in these pools known. The ferric ions in the Fe^{III} nanoparticles found in Atm1-depleted mitochondria appear to be coordinated by ligands with oxygen donors but essentially lacking in N, S or C atoms (41). Phosphate, water and hydroxide ligands were suggested as likely ligands in these nanoparticles, and similar ligands might be associated with the nanoparticles observed in mitochondria from WT fermenting cells. The nonheme high-spin Fe^{II} pool may consist of multiple species. Some mitochondrial proteins (e.g. frataxin, ferrochelatase, Fe/S cluster scaffold proteins, CoQ7) may coordinate HS Fe^{II} ions, but the collective concentration of these proteins may be insufficient to account for the overall concentration of the NHHS Fe^{II} pool (*ca*. 150 μM in fermenting mitochondria). Seguin *et al*. (42) determined that yeast cells grown under similar conditions contained ~ 1300 copies of Yfh1p. If we assume 60×10^{-15} L for the volume of a yeast cell(43–46), and that 3% of that volume were due to mitochondria (47–48), and that each Yfh1p bound 2 Fe^{II} ions (49), this would correspond to a concentration of ~ 70 nM. Even if there were a dozen such proteins in mitochondria, their collective concentration would be two orders of magnitude less than that present in the NHHS Fe^{II} pool of fermenting mitochondria. These considerations strongly suggest that *the nonheme HS* Fe^{II} *pool is dominated by non-proteinaceous low-molecular weight complexes*.

The results of this study can be compared to proteomic studies that also indicate substantial changes in the yeast mitochondria proteome due to the diauxic shift (23). The concentrations of 17 proteins are significantly lower in fermenting *vs*. respiring cells including cytochrome *c* oxidase, cytochrome bc_1, and succinate dehydrogenase (50). The mitochondrial transcriptome changes more dramatically, with transcripts of cytochrome *c* isoform 1 and Mn-superoxide dismutase (MnSod2) declining under fermentation (51–52). Other groups have also reported lower SOD2 protein and transcript levels under fermentation (53–54). Our results are consistent, including the 3-fold increase in the Mn concentration of respiring mitochondria relative to respiro-fermenting and fermenting conditions which might reflect changes in the levels of MnSod2 or associated Mn species.

The observed changes in the distribution of Fe in mitochondria isolated from cells grown under different metabolic modes can be interpreted given the known roles of mitochondria in respiring *vs*. fermenting cells. In respiring cells, these organelles are critical for energy production, which requires the biosynthesis of Fe/S clusters and heme centers, as well as their installation into apo-respiratory complexes. Under fermentation conditions, energy production is associated with glycolysis, where no such centers are involved. Thus, *the production of Fe/S clusters and heme centers is probably reduced in fermenting mitochondria because the metabolic need for these centers is reduced.* Our results suggest a 3-fold reduction in these centers. Residual amounts of such centers might allow fermenting cells to convert rapidly into respiration mode as environmental conditions change.

The Fe used to synthesize mitochondrial Fe/S clusters and hemes is imported into the organelle as Fe^{II} (55). Neither the structure nor composition of the imported complex(es) are known but they are probably of low molecular weight as they must pass through transporters in the IM (3). *We propose that the nonheme HS Fe^{II} ions present in fermenting mitochondria are these imported ions and that they serve in this capacity.* The simple model of Figure 8 assumes this role and can rationalize the observed changes in the level of this pool. During respiration, the size of the Fe^{II} pool is small since the biosynthesis rates of Fe/S clusters and hemes are elevated. During fermentation, the pool increases because the rate of Fe/S cluster and heme biosynthesis is diminished. Consistent with the nearly invariant Fe concentrations in respiring and fermenting mitochondria, the overall rate of Fe^{II} import appears to be unaffected by changes in metabolic growth mode; i.e. *the cell does not seem to regulate the rate of Fe^{II} import into mitochondria according to metabolic growth mode.* Understanding Fe fluxes at the cellular level will require that the different percentage volumes occupied by mitochondria in fermenting *vs*. respiring cells be taken into account. Another uncertainty, at the mitochondrial level, is the relationship between the NHHS Fe^{II} pool and the other pools of Fe in fermenting mitochondria, including Fe^{III} nanoparticles, mononuclear HS Fe^{III} ions, and the central unresolved material. The three pools may exist in a dynamic equilibrium with each other or they might be independent (e.g. imported by different IM transporters). Also uncertain is the cellular *function* of these other pools. They certainly *store* Fe in fermenting mitochondria, and the absence of these pools during respiration suggests either that these pools can be utilized under respiratory growth conditions or that they never form under these conditions. However, whether this is a cellular *strategy* for storing Fe, analogous to mitoferrin in human mitochondria (56), is uncertain. These pools may possibly result from an insufficient concentration of a coordinating ligand or to a shift of either pH or oxidation status in fermenting mitochondria. We favor this latter characterization especially for the Fe^{III} nanoparticle pool, in that the ligands coordinating these ions are probably not protein bound and thus would not be under the direct genetic control of the cell. Nevertheless, this pool may indirectly impact cellular function, e.g. by generating reactive oxygen species during its formation, and it may be bioavailable under particular metabolic conditions.

Supplementary Material

Refer to Web version on PubMed Central for supplementary material.

Acknowledgments

We thank Dr. Graham Palmer (Rice University) for generously providing a digital spectrum of cytochrome *c* oxidase and Dr. Carla Koehler (University of California, Los Angeles) for kindly providing the cytochrome *c* antibody.

Abbreviations

HS	high-spin
LS	low-spin, NHHS, nonheme high-spin
IM	inner membrane
EPR	electron paramagnetic resonance, ICP-MS, inductively coupled plasma emission mass spectrometry

References

1. Hudder BN, Morales JG, Stubna A, Münck E, Hendrich MP, Lindahl PA. Electron paramagnetic resonance and Mössbauer spectroscopy of intact mitochondria from respiring *Saccharomyces cerevisiae*. Journal of Biological Inorganic Chemistry. 2007; 12:1029–1053. [PubMed: 17665226]
2. Lindahl PA, Morales JG, Miao R, Holmes-Hampton G. Chapter 15 Isolation of Saccharomyces cerevisiae mitochondria for Mössbauer, EPR, and electronic absorption spectroscopic analyses. Methods Enzymol. 2009; 456:267–285. [PubMed: 19348894]
3. Lill R, Muhlenhoff U. Maturation of iron-sulfur proteins in eukaryotes: Mechanisms, connected processes, and diseases. Annu Rev Biochem. 2008; 77:669–700. [PubMed: 18366324]
4. Beinert H. Spectroscopy of succinate dehydrogenases, a historical perspective. Biochimica Et Biophysica Acta-Bioenergetics. 2002; 1553:7–22.
5. Hunte C, Koepke J, Lange C, Rossmanith T, Michel H. Structure at 2.3 angstrom resolution of the cytochrome bc(1) complex from the yeast *Saccharomyces cerevisiae* co-crystallized with an antibody Fv fragment. Structure. 2000; 8:669–684. [PubMed: 10873857]
6. Beinert H, Shaw RW. On Identitiy of High-Spin Heme Components of Cytochrome-C Oxidase. Biochimica et Biophysica Acta. 1977; 462:121–130. [PubMed: 199250]
7. Barrientos A. Yeast Models of Human Mitochondrial Diseases. IUBMB Life. 2003; 55:85–95.
8. Irazusta V, Moreno-Cermeño A, Cabiscol E, Ros J, Tamarit J. Major targets of iron-induced protein oxidative damage in frataxin-deficient yeasts are magnesium-binding proteins. Free Radic Biol Med. 2008; 44:1712–1723. [PubMed: 18280258]
9. Rouault TA, Tong W-H. Iron–sulfur cluster biogenesis and human disease. Trends Genet. 2008; 24:398–407. [PubMed: 18606475]
10. Veatch JR, McMurray MA, Nelson ZW, Gottschling DE. Mitochondrial Dysfunction Leads to Nuclear Genome Instability via an Iron-Sulfur Cluster Defect. Cell. 2009; 137:1247–1258. [PubMed: 19563757]
11. Huang ME, Kolodner RD. A biological network in Saccharomyces cerevisiae prevents the deleterious effects of endogenous oxidative DNA damage. Molecular Cell. 2005; 17:709–720. [PubMed: 15749020]
12. Barja, G. Mitochondrial free radical production and aging in mammals and birds. Harman, D.; Holliday, R.; Meydani, M., editors. New York: Acad Sciences; 1998. p. 224-238.
13. Raha S, McEachern GE, Myint AT, Robinson BH. Superoxides from mitochondrial complex III: The role of manganese superoxide dismutase. Free Radic Biol Med. 2000; 29:170–180. [PubMed: 10980405]

14. Turrens JF. Superoxide production by the mitochondrial respiratory chain. Biosci Rep. 1997; 17:3–8. [PubMed: 9171915]
15. Scheffler, IE. Mitochondria. Wiley-Liss; New York, New York: 1999.
16. Babcock M, deSilva D, Oaks R, DavisKaplan S, Jiralerspong S, Montermini L, Pandolfo M, Kaplan J. Regulation of mitochondrial iron accumulation by Yfh1p, a putative homolog of frataxin. Science. 1997; 276:1709–1712. [PubMed: 9180083]
17. Carraway MS, Suliman HB, Madden MC, Piantadosi CA, Ghio AJ. Metabolic capacity regulates iron homeostasis in endothelial cells. Free Radic Biol Med. 2006; 41:1662–1669. [PubMed: 17145554]
18. Lesuisse E, Santos R, Matzanke BF, Knight SAB, Camadro JM, Dancis A. Iron use for haeme synthesis is under control of the yeast frataxin homologue (Yfh1). Hum Mol Genet. 2003; 12:879–889. [PubMed: 12668611]
19. Napoli E, Taroni F, Coropassi GA. Frataxin, Iron–Sulfur Clusters, Heme, ROS, and Aging. Antioxidants and Redox Signaling. 2006; 8:506–516. [PubMed: 16677095]
20. Hare D, Reedy B, Grimm R, Wilkins S, Volitakis I, George JL, Cherny RA, Bush AI, Finkelstein DI, Doble P. Quantitative elemental bio-imaging of Mn, Fe, Cu and Zn in 6-hydroxydopamine induced Parkinsonism mouse models. Metallomics. 2009; 1:53–58.
21. Lee DW, Kaur D, Chinta SJ, Rajagopalan S, Andersen JK. A Disruption in Iron-Sulfur Center Biogenesis via Inhibition of Mitochondrial Dithiol Glutaredoxin 2 May Contribute to Mitochondrial and Cellular Iron Dysregulation in Mammalian Glutathione-Depleted Dopaminergic Cells: Implications for Parkinson's Disease. Antioxid Redox Signaling. 2009; 11:2083–2094.
22. Camaschella C, Campanella A, De Falco L, Boschetto L, Merlini R, Silvestri L, Levi S, Iolascon A. The human counterpart of zebrafish shiraz shows sideroblastic-like microcytic anemia and iron overload. Blood. 2007; 110:1353–1358. [PubMed: 17485548]
23. Schonauer MS, Dieckmann CL. Mitochondrial genomics and proteomics. Curr Genomics. 2004; 5:575–588.
24. Münck E, Sidney F, Lester P. Mossbauer spectroscopy of proteins: Electron carriers. Methods in Enzymology Volume. 1978; 54:346–379.
25. Stevens BJ. Variation in Number and Volume of Mitochondria in Yeast According to Growth-Conditions - Study Based on Serial Sectioning and Computer Graphics Reconstitution. Biologie Cellulaire. 1977; 28:37–56.
26. Egner A, Jakobs S, Hell SW. Fast 100-nm resolution three-dimensional microscope reveals structural plasticity of mitochondria in live yeast. Proc Natl Acad Sci U S A. 2002; 99:3370–3375. [PubMed: 11904401]
27. Miao R, Martinho M, Morales JG, Kim H, Ellis EA, Lill R, Hendrich MP, Munck E, Lindahl PA. EPR and Mossbauer spectroscopy of intact mitochondria isolated from Yah1p-depleted Saccharomyces cerevisiae. Biochemistry. 2008; 47:9888–9899. [PubMed: 18717590]
28. Sherman F. Getting Started with Yeast. Methods in Enzymology. 1991; 194:3–21. [PubMed: 2005794]
29. Holmes-Hampton GP, Miao R, Garber-Morales J, Guo Y, Münck E, Lindahl PA. A nonheme high-spin ferrous pool in mitochondria from fermenting *Saccharomyces cerevisiae*. Biochemistry. 2010; 49:4227–4234. [PubMed: 20408527]
30. Dabir DV, Leverich EP, Kim SK, Tsai FD, Hirasawa M, Knaff DB, Koehler CM. A role for cytochrome c and cytochrome c peroxidase in electron shuttling from Erv1. Embo J. 2007; 26:4801–4811. [PubMed: 17972915]
31. Cobine PA, Ojeda LD, Rigby KM, Winge DR. Yeast contain a non-proteinaceous pool of copper in the mitochondrial matrix. J Biol Chem. 2004; 279:14447–14455. [PubMed: 14729672]
32. Foury F, Cazzalini O. Deletion of the yeast homologue of the human gene associated with Friedreich's Ataxia elicits iron accumulation in mitochondria. FEBS Lett. 1997; 411:373–377. [PubMed: 9271239]
33. Kispal G, Csere P, Prohl C, Lill R. The mitochondrial proteins Atm1p and Nfs1p are essential for biogenesis of cytosolic FeS proteins. Embo J. 1999; 18:3981–3989. [PubMed: 10406803]

34. Tangeras A, Flatmark T, Backstrom D, Ehrenberg A. Mitochondrial Iron Not Bound in Heme and Iron-Sulfur Centers - Estimation, Compartmentation and Redox State. Biochimica et Biophysica Acta. 1980; 589:162–175. [PubMed: 6243966]
35. Liao GL, Palmer G. The reduced minus oxidized difference spectra of cytochromes a and a(3). Biochimica et Biophysica Acta-Bioenergetics. 1996; 1274:109–111.
36. Wang H, Sauke T, Debrunner PG, Chan SI. The CO Adduct of Yeast Cytochrome-C Oxidase - Mössbauer and Photolysis Studies. J Biol Chem. 1988; 263:15260–15263. [PubMed: 2844807]
37. Pikus JD, Studts JM, Achim C, Kauffmann KE, Munck E, Steffan RJ, McClay K, Fox BG. Recombinant toluene-4-monooxygenase: Catalytic and Mössbauer studies of the purified diiron and Rieske components of a four-protein complex. Biochemistry. 1996; 35:9106–9119. [PubMed: 8703915]
38. Maguire JJ, Johnson MK, Morningstar JE, Ackrell BAC, Kearney EB. Electron-Paramagnetic Rresonance Studies of Mammalian Succinate-Dehyrogenase Detection of the Tetranuclear Cluster S2. J Biol Chem. 1985; 260:909–912.
39. Fee JA, Findling KL, Yoshida T, Hille R, Tarr GE, Hearshen DO, Dunham WR, Day EP, Kent TA, Munck E. Purification and Characterization of the Rieske Iron-Sulfur Protein from *Thermus-Thermophilus* - Evidence for a [2Fe-2S] Cluster Having Non-Cysteine Ligands. J Biol Chem. 1984; 259:124–133. [PubMed: 6323399]
40. Swanson MA, Usselman RJ, Frerman FE, Eaton GR, Eaton SS. The iron-sulfur cluster of electron transfer flavoprotein-ubiquinone oxidoreductase is the electron acceptor for electron transfer flavoprotein. Biochemistry. 2008; 47:8894–8901. [PubMed: 18672901]
41. Miao R, Kim H, Koppolu UMK, Ellis EA, Scott RA, Lindahl PA. Biophysical Characterization of the Iron in Mitochondria from Atm1p-Depleted *Saccharomyces cerevisiae*. Biochemistry. 2009; 48:9556–9568. [PubMed: 19761223]
42. Seguin A, Bayot A, Dancis A, Rogowska-Wrzesinska A, Auchere F, Camadro JM, Bulteau AL, Lesuisse E. Overexpression of the yeast frataxin homolog (Yfh1): Contrasting effects on iron-sulfur cluster assembly, heme synthesis and resistance to oxidative stress. Mitochondrion. 2009; 9:130–138. [PubMed: 19460301]
43. Jorgensen P, Nishikawa JL, Breitkreutz BJ, Tyers M. Systematic identification of pathways that couple cell growth and division in yeast. Science. 2002; 297:395–400. [PubMed: 12089449]
44. Sherman, F. Guide to Yeast Genetics and Molecular and Cell Biology. 2002. Getting started with yeast; p. 3-41.
45. Tamaki H, Yun CW, Mizutani T, Tsuzuki T, Takagi Y, Shinozaki M, Kodama Y, Shirahige K, Kumagai H. Glucose-dependent cell size is regulated by a G protein-coupled receptor system in yeast Saccharomyces cerevisiae. Genes to Cells. 2005; 10:193–206. [PubMed: 15743410]
46. Tyson CB, Lord PG, Wheals AE. Dependency of Size of *Saccharomyces cerevisiae* Cells on Growth-Rate. Journal of Bacteriology. 1979; 138:92–98. [PubMed: 374379]
47. Polakis ES, Bartley W, Meek GA. Changes in Structure + Enzyme Activity of Saccharomyces Cerevisiae in Response to Changes in Environment. Biochem J. 1964; 90:369. [PubMed: 4284219]
48. Polakis ES, Bartley W, Meek GA. Changes in Activities of Respiratory Enzymes during Aerobic Growth of Yeast on Different Carbon Sources. Biochem J. 1965; 97:298. [PubMed: 16749117]
49. Cook JD, Bencze KZ, Jankovic AD, Crater AK, Busch CN, Bradley PB, Stemmler AJ, Spaller MR, Stemmler TL. Monomeric yeast frataxin is an iron-binding protein. Biochemistry. 2006; 45:7767–7777. [PubMed: 16784228]
50. Ohlmeier S, Kastaniotis AJ, Hiltunen JK, Bergmann U. The Yeast Mitochondrial Proteome, a Study of Fermentative and Respiratory Growth. J Biol Chem. 2004; 279:3956–3979. [PubMed: 14597615]
51. Costa V, Amorim MA, Reis E, Quintaniha A, Moradas-Ferreira P. Mitochondrial superoxide dismutase is essential for ethanol tolerance of *Saccharomyces cerevisiae* in the post-diauxic phase. Microbiology. 1979; 143:1649–1656. [PubMed: 9168613]
52. Zitomer RS, Montgomery DL, Nichols DL, Halo BD. Transcriptional regulation of the yeast cytochrome c gene. Proc Natl Acad Sci U S A. 1979; 76:3627–3631. [PubMed: 226972]

53. Macierzynska E, Grzelak A, Bartosz G. The effect of growth medium on the antioxidant defense of Saccharomyces cerevisiae. Cellular & Molecular Biology Letters. 2007; 12:448–456.

54. Maris AF, Assumpcao ALK, Bonatto D, Brendel M, Henriques JAP. Diauxic shift-induced stress resistance against hydroperoxides in Saccharomyces cerevisiae is not an adaptive stress response and does not depend on functional mitochondria. Current Genetics. 2001; 39:137–149. [PubMed: 11409175]

55. Lange H, Kispal G, Lill R. Mechanism of iron transport to the site of heme synthesis inside yeast mitochondria. J Biol Chem. 1999; 274:18989–18996. [PubMed: 10383398]

56. Paradkar PN, Zumbrennen KB, Paw BH, Ward DM, Kaplan J. Regulation of Mitochondrial Iron Import through Differential Turnover of Mitoferrin 1 and Mitoferrin 2. Mol Cell Biol. 2009; 29:1007–1016. [PubMed: 19075006]

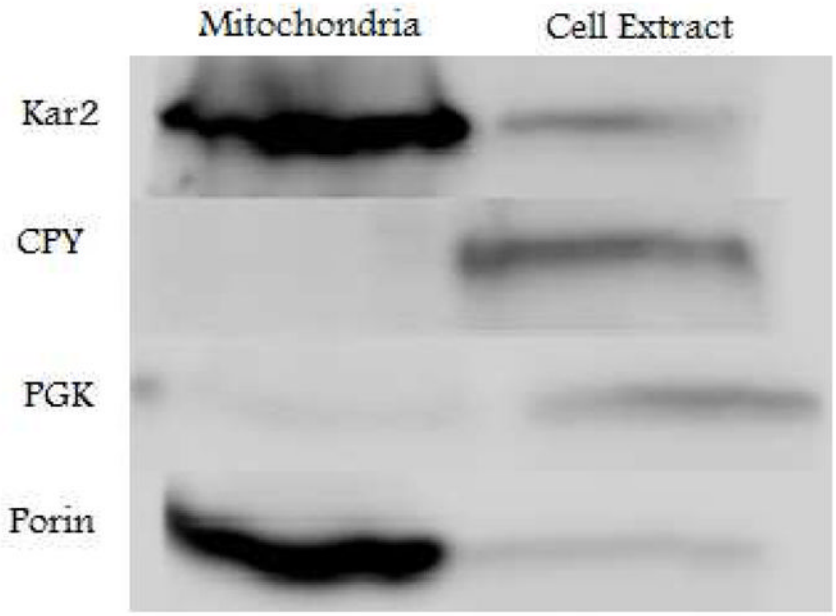

Figure 1.
Western blot of EGTA-washed isolated mitochondria (left lane) and corresponding extract (right lane) from respiring cells (Batch R5). In both cases 60 μg of protein were loaded into the wells of a 10% SDS-PAGE gel. Kar2 is an endoplasmic reticular protein (5× increased in isolated mitochondria vs. cell extract); CPY is a vacuolar protein (6× decreased); PGK is a cytosolic protein (5× decreased); Porin is a mitochondrial protein (10× increased).

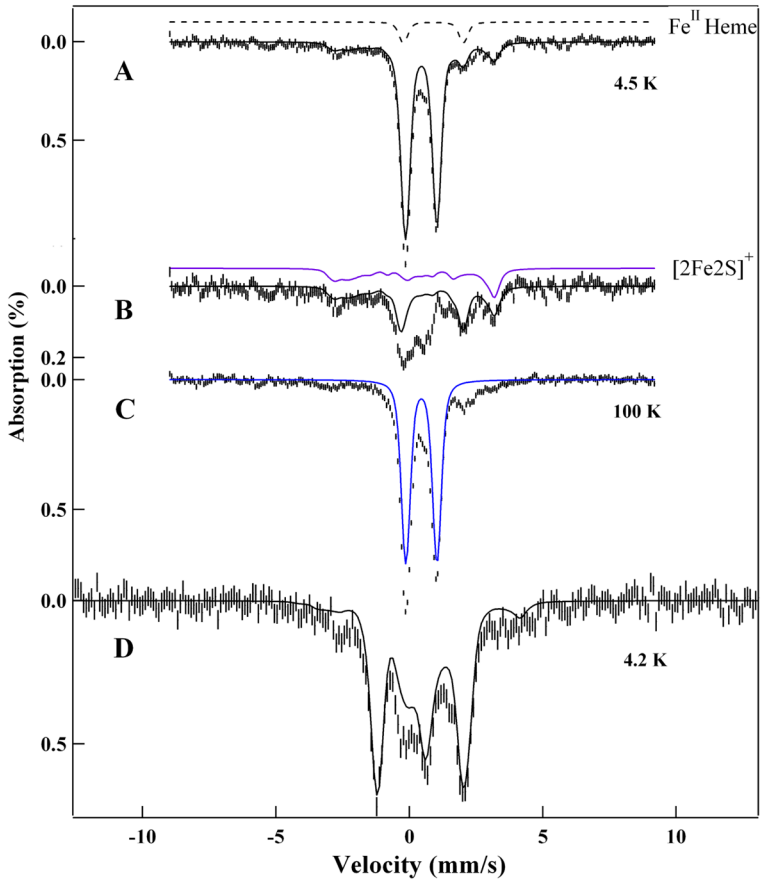

Figure 2.

Mössbauer Spectra of packed mitochondria (batch R1) isolated from respiring cells. A, 4.5 K, 0.05 T field applied parallel to the γ radiation. The black line is a simulation for the sum of the central doublet, HS Fe^{II} hemes (dashed), and S = ½ $[Fe_2S_2]^{1+}$ clusters. See Table 1 and bar graph (Figure 7) for percentages for all components. B, same as A after subtracting the central doublet and HS Fe^{II} heme contributions. The purple solid line is a simulation for S = ½ $[Fe_2S_2]^{1+}$ clusters, while the black solid line is a composite simulation including these species and HS Fe^{II} hemes. The absorption between 0 and + 1 mm/s that is not covered by the black curve is unassigned. C, same as A but recorded at 100 K. The blue line outlines the contribution of the central doublet in the sample. D, same as A except with 8.0 T parallel applied field. The black line is a simulation that includes the central doublet and contributions from S = ½ $[Fe_2S_2]^{1+}$ clusters.

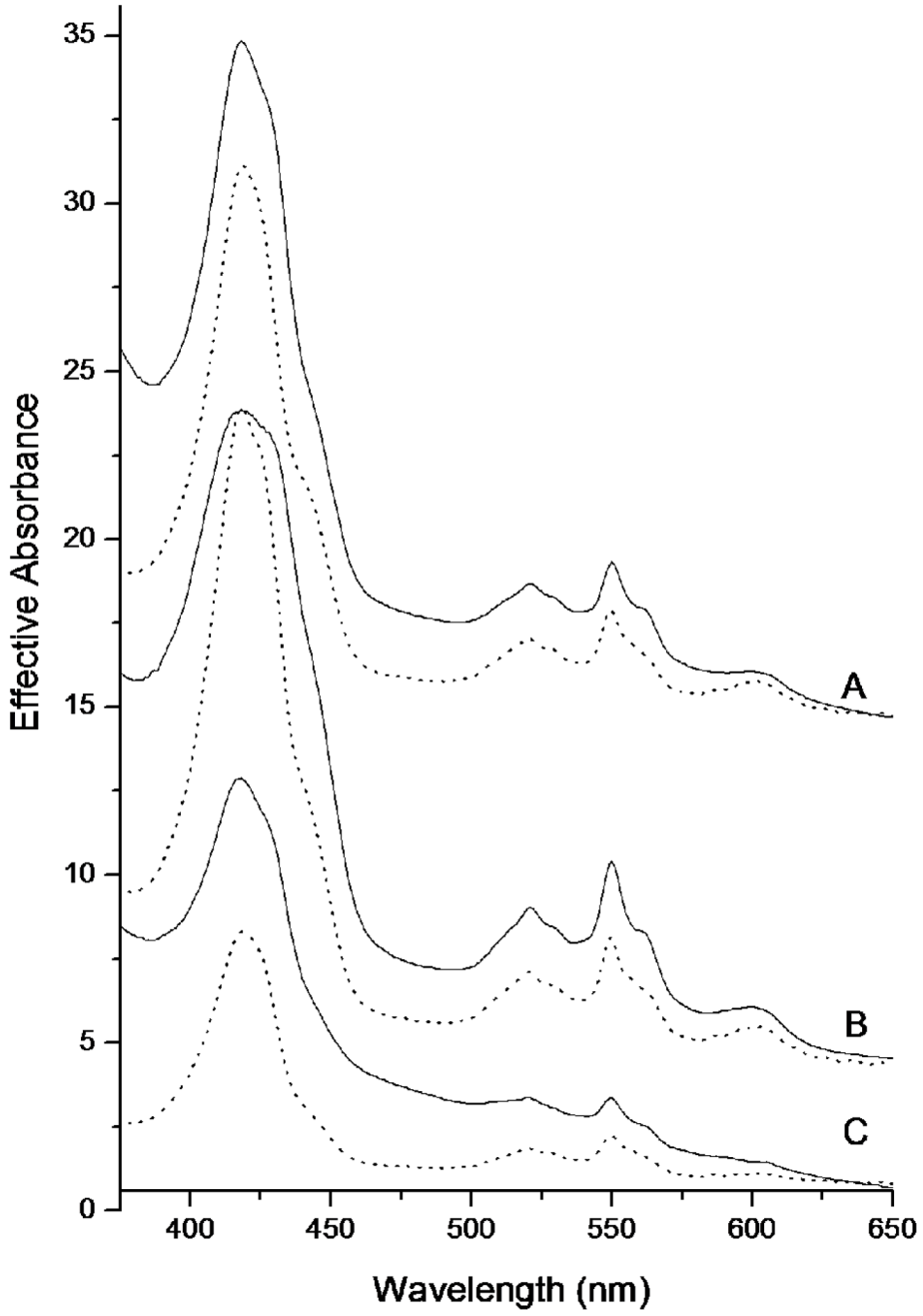

Figure 3.

Electronic Absorption spectra of mitochondrial suspensions. A, respiring (R1); B, respiro-fermenting (RF2); C, fermenting (F3). Effective absorbances of neat mitochondria normalized to a 10 mm pathlength cuvette are plotted. These values were obtained by multiplying raw absorbances by 2.0 (the dilution factor relative to packed mitochondria) and 5.0 (pathlength factor due to the use of a 2 mm pathlength cuvette), and by dividing by 0.82 (the packing factor). Dashed lines are composites from individual heme *a*, *b*, and *c* containing proteins, using parameters given in Table S1 (averages in Table 1).

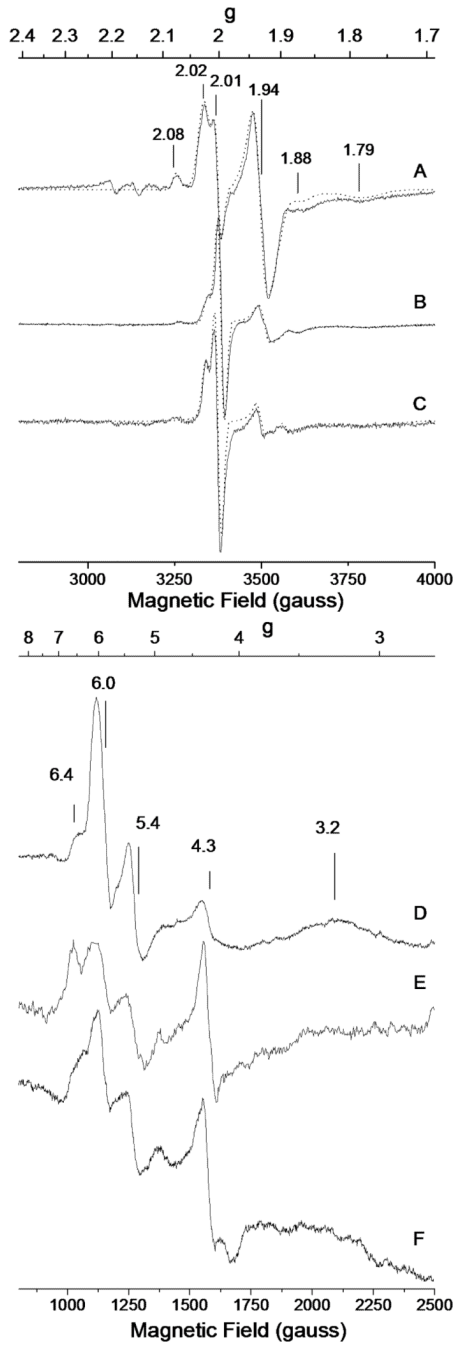

Figure 4.

10 K EPR spectra of mitochondria from respiring (A, batch R2, decomposition in S5), respiro-fermenting (B, RF1), and fermenting (C, F11) cells. Spectra A and C were collected at 0.05 mW, spectrum B at 0.2 mW. Dashed lines are simulations, with batch-averaged parameters given in Table 1. D, E and F are the low-field regions of A, B and C, respectively.

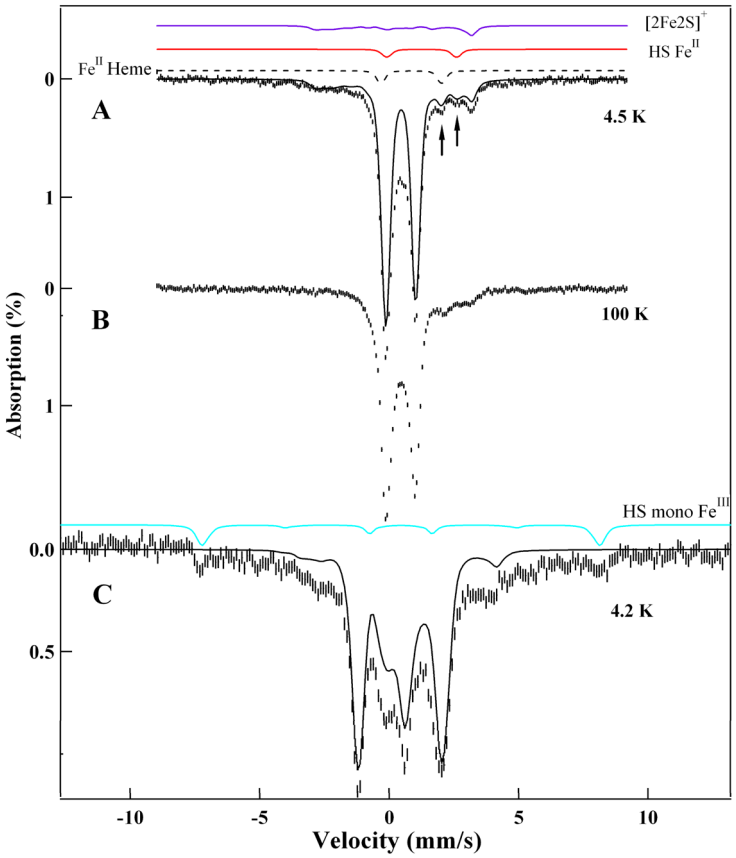

Figure 5.

Mössbauer spectra of packed mitochondria (RF1) from respiro-fermenting cells. A, Spectrum measured at 4.5 K, 0.05 T parallel applied field. The black line is a simulation for the central doublet, HS Fe^{II} hemes, NHHS Fe^{II}, and S = ½ $[Fe_2S_2]^{1+}$ clusters. The lines above the spectrum are simulations for S = ½ $[Fe_2S_2]^{1+}$ (purple), nonheme HS Fe^{II} (red) and the HS Fe^{II} hemes (black dashed line). B, same as A but at 100 K. C, same as A but at 8.0 T. The black line is a simulation for the central doublet and S = ½ $[Fe_2S_2]^{1+}$ clusters. The cyan line above is a simulation for HS mononuclear Fe^{III} species.

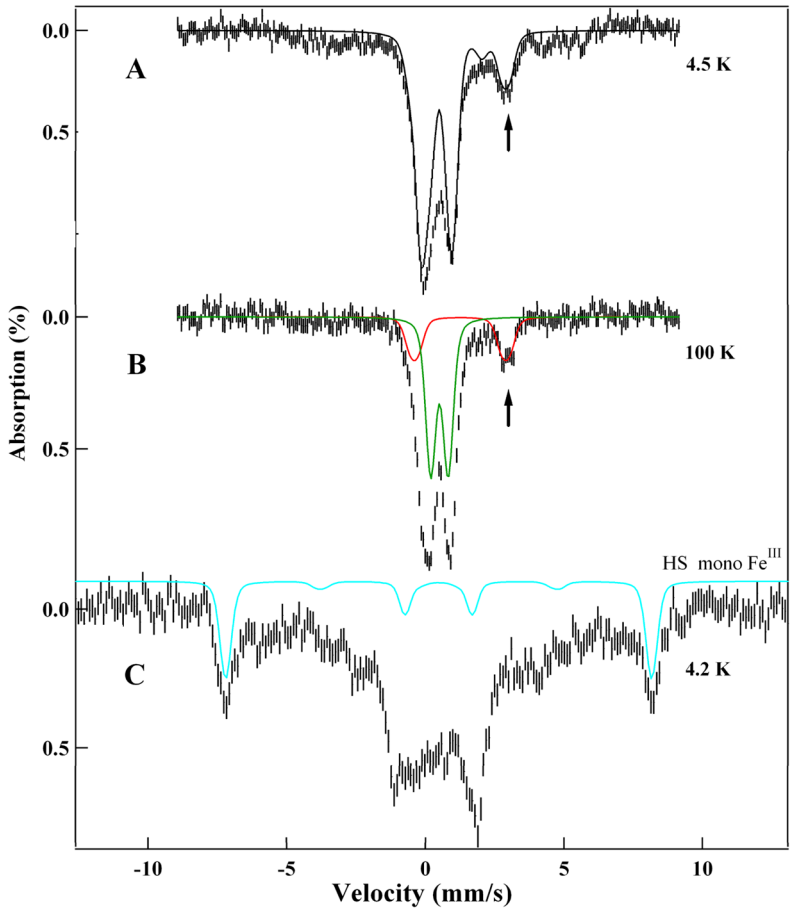

Figure 6.

Mössbauer spectra of mitochondria (batch F9) from fermenting cells. A, 4.5 K, 0.05 T parallel applied magnetic field. The black line is a simulation for the sum of the central doublet, HS Fe^{II} hemes, NHHS Fe^{II} (high-energy line indicated by arrow), and the Fe^{III} nanoparticles. B, same as A except at 100 K. The red line indicates HS Fe^{II}; green line indicates nanoparticle contribution. C, same as A except at 8.0 T. The cyan line is a simulation for the HS Fe^{III}.

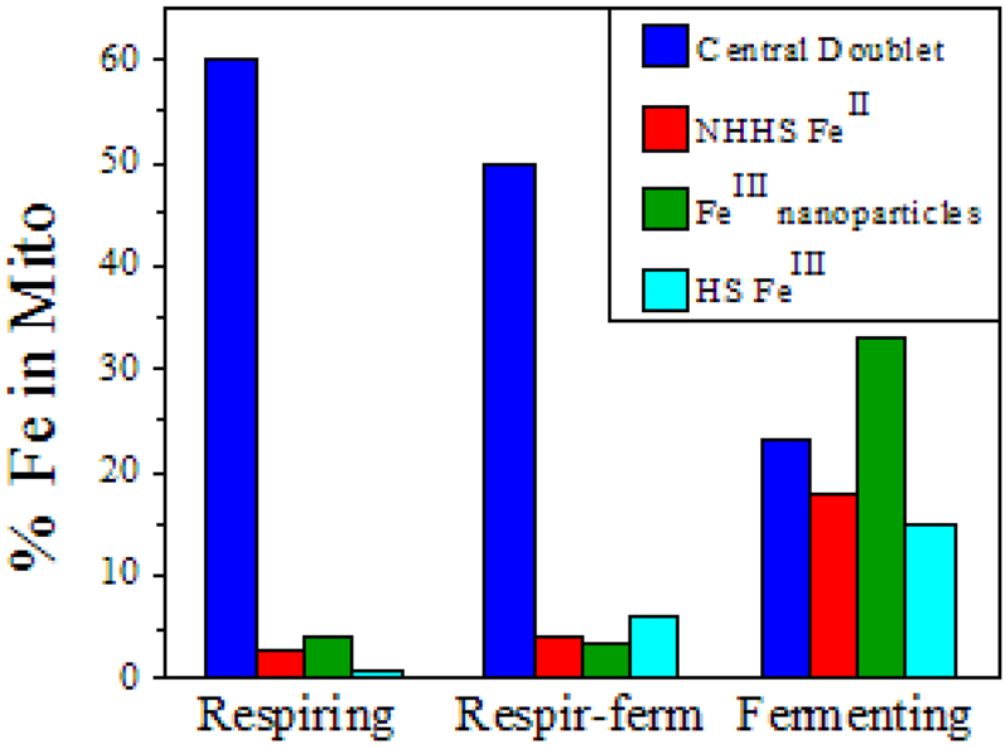

Figure 7.
Bar graph showing the major forms of Fe present in respiring, respiro-fermenting, and fermenting mitochondria. Color-coding is matched to simulated features in previous figures.

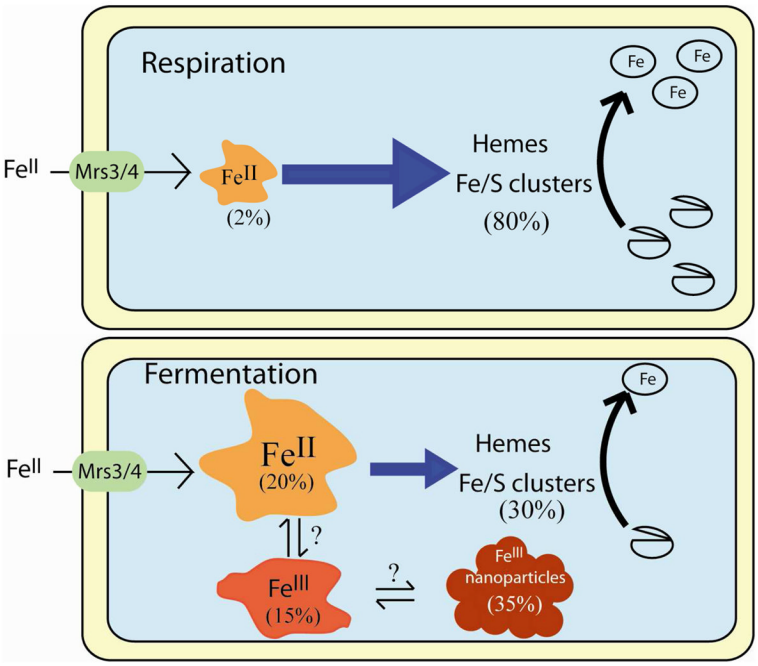

Figure 8.

Model describing the shift in the iron content of mitochondria with metabolic growth mode. The size of the NHHS Fe^{II} pool is dictated by the balance of input and output fluxes. During respiration, the pool is small (~ 15 μM). When cells ferment, the rate of Fe/S cluster and heme biosynthesis declines, causing the pool to enlarge (~ 150 μM). The rate of Fe^{II} import from the cytosol is not significantly affected by the change in metabolism. Under fermenting conditions, a portion of the NHHS Fe^{II} pool may become oxidized to mononuclear nonheme HS Fe^{III}, a subset of which may precipitate as Fe^{III} nanoparticles.

Table 1

Analytical properties of isolated mitochondria[a]

	Respiring	Respiro-fermenting	Fermenting
Protein (mg/mL)	170 ± 61 (5)	200 ± 60 (2)	110 ± 30 (11)
Fe (μM)	720 ± 210 (5)	840 ± 120 (2)	770 ± 320 (11)
Cu (μM)	210 ± 170 (5)	160 ± 80 (2)	50 ± 37 (11)
Mn (μM)	35 ± 20 (5)	12 ± 4 (2)	15 ± 12 (11)
Zn (μM)	290 ± 160 (5)	230 ± 150 (2)	290 ± 210 (11)
Central Doublet	60 ± 2% (2)	50% (1)	25 ± 4% (5)
HS Fe^{II} heme	7 ± 1% (2)	4% (1)	4 ± 1% (5)
NHHS Fe^{II}	2 ± 1% (2)	3% (1)	20 ± 5% (5)
HS Fe^{III}	0 (2)	5% (1)	15 ± 3% (3)
S = ½ $[Fe_2S_2]^{1+}$	13 ± 2% (2)	10% (1)	~ 0% (5)
$[Fe_2S_2]^{2+}$	< 5% (2)	< 5% (1)	~ 0% (5)
Fe^{III} nanoparticles	< 5% (2)	< 5% (1)	33 ± 7% (5)
unassigned Fe	~20%	~25%	~5% (5)
Fe^{II} Heme *a*(μM)	51 ± 8 (4)	61 (1)	14 ± 1 (4)
Fe^{II} Heme *b*(μM)	52 ± 8 (4)	55 (1)	27 ± 5 (4)
Fe^{II} Heme *c*(μM)	120 ± 10 (4)	160 (1)	73 ± 15 (4)
g_{ave} = 1.94 (μM)	1 – 10 (3)	13 ± 4 (2)	1 – 3 (2)
g_{ave} = 1.90 (μM)	13 ± 3 (3)	29 ± 18 (2)	6 ± 2 (2)
g = 2.01 (μM)	0 – 1 (3)	1 – 2 (2)	0 (2)
g = 2.00 (μM)	0 – 2 (3)	0 – 6 (2)	0 – 1 (2)
g = 2.04 (μM)	1 – 3 (3)	3 ± 1 (2)	1 – 2 (2)
g = 4.3 (μM)	5 – 45 (3)	2 – 14 (2)	3 (1)
g = 5.8 (μM)	1 – 2 (3)	0 – 2 (2)	~ 0 (1)
g = 6.4, 5.3(μM)	1 – 4 (3)	0 – 5 (2)	1 (1)
Cytochrome c oxidase	30	35	8
Succinate dehydrogenase	5	10	2
Cytochrome bc_1	10	20	6
Cytochrome *c*	100	140	60
Other HS heme *b*	20	Minor	minor
Other LS hemes combined	180	230	100
Other $[Fe_4S_4]^{2+}$ only	55	36	13
Other $[Fe_4S_4]^{2+}$ + $[Fe_2S_2]^{+}$	Minor	Minor	minor
Other $[Fe_2S_2]^{2+}$ only	Minor	Minor	minor
Cu^{I} Pool	120	60	30

[a]Top Panel; concentrations are for “neat” mitochondria (devoid of residual interstitial solvent). Experimentally determined protein and metal concentrations of mitochondrial suspensions were multiplied by the dilution factor used to prepare these samples from the packed state.

Concentrations were also divided by 0.82, the packing efficiency (1–2). Values in the table are the *average* of the individual determinations given in Table S1; the number of samples evaluated is in parentheses. Indicated relative uncertainties reflect variations between samples; additional uncertainties related to fitting are estimated to be ± 20%. Heme *a*, *b*, and *c* concentrations were determined from electronic absorption spectra.

Entries obtained by Mössbauer spectroscopy are given in % of total Fe. Percentages of HS Fe^{III} species were determined only from 8.0 T Mössbauer spectra. Bottom Panel; estimated concentrations of dominating Fe- and Cu-containing species in yeast mitochondria (in μM).